MATERIALS PHYSICS AND MECHANICS RESEACH ARTICLE

Submitted: March 14, 2024 **Revised: May 29, 2024** **Accepted: July 16, 2024**

Experimental determination of physical, chemical and surface properties of biocompatible thermoplastic

D.A. Erofeev [1], P.B. Pirozhnikov [1], I.A. Keresten [2]✉, A.G. Titov [3]

[1] St. Petersburg Institute of Technology (Technical University), St. Petersburg, Russia

[2] Peter the Great St. Petersburg Polytechnic University, St. Petersburg, Russia

[3] Institute of Medical Education of Almazov National Medical Research Centre, St. Petersburg, Russia

✉ keresten@compmechlab.com

ABSTRACT

The main purpose of this research is determination of physical, chemical and surface properties of thermoplastics, which were certificated for medical employment, for implant or prosthesis manufacturing. The physical and chemical structure of thermoplastics (polyacrylonitrile-co-butadiene-co-styrene, polycarbonate, polyetherimide) were investigated with the Fourier-transform infrared spectroscopy (FTIR), differential thermal and thermogravimetric analysis (DTA/TG), differential scanning calorimetry (DSC), wide-angle X-ray diffraction (XRD) and scanning electron microscopy (SEM). The surface of all investigated thermoplastics had a transition or a hydrophobic state. The contact angle hysteresis by distilled water was in range 95.6–103.0° that indicates sticky wetting behavior of surfaces. The contact angle by blood plasma was in the range 84.7–92.1°, depending on the chemical structure of the thermoplastic polymer. Despite the lower contact angle value of the blood plasma, the amount of its adsorption was greater than in case of distilled water, and it should be considered in development of medical polymer devices.

KEYWORDS

thermoplastics • polyacrylonitrile-co-butadiene-co-styrene • polycarbonate • polyetherimide • endoprosthetics physical and chemical properties • surface wetting

Citation: Erofeev DA, Pirozhnikov PB, Keresten IA, Titov AG. Experimental determination of physical, chemical and surface properties of biocompatible thermoplastic. *Materials Physics and Mechanics*. 2024;52(3): 1–12. http://dx.doi.org/10.18149/MPM.5232024_1

Introduction

Endoprosthetics is the widespread surgical procedure for normal function recovery of original joints after different defects or diseases [1]. The Increase of the joint's replacement surgery is conditioned by both a growth of average life expectancy and an implant service time (more than 12–15 years) due to the appearance of new materials [2]. Usually for implant production the titanium alloy Ti_6Al_4V is used as base material, because it contains a whole set of required properties for medical devices (a biocompatibility, an ultimate strength, etc.). Unfortunately, the usage of Ti_6Al_4V in the musculoskeletal system may lead to bone tissue destruction near the contact surface of bone-implant pairs for two reasons. Firstly, due to the difference in mechanical properties between the cortical bone and Ti_6Al_4V [3,4]. Secondly, the contact surface of the bone-implant pair includes screw holes for its connection, which represent a stress concentrator and lead to increase the stress and probability of bone failure [5–7]. In addition, it is necessary to identify the shape of the implant for greater compatibility of bone-implant contact pair, which leads to increasing the implant lifetime and shortening the period of patient rehabilitation after

the surgery. Today it is possible to manufacture personalized implants which consider individual patient's characteristics which are obtained using computerized tomography. However, standard-size implants are still used because personalized implants have a longer production cycle. Unfortunately, standard-size implants consider individual characteristics of the patient only partially, which lead to shortening the implant lifetime due to imperfect contact interaction [1].

A more complicated situation occurred with the revision of endoprosthetics. Standard-size metallic implants often have a polygonal shape that can lead to several problems. Firstly, it will require excessive bone removing for a precise augment placing. Secondly, the unrounded shape corners will be zones with increased mechanical stress, which lead to the bone tissue destruction. Therefore, it is crucial to simplify and shorten the production cycle of implants with complicated shapes (for example, it would be quite convenient to manufacture implants "near operating table") to increase the implant lifetime and to shorten the period of patient rehabilitation after the surgery. For such purpose, thermosetting polymers are more preferred for manufacturing implants with complicated shapes.

Polymeric materials can be very useful as polymer matrix composite for different kinds of medical devices (implants, prostheses, syringes, blood bags and other) [8]. Medical devices, which are made of polymeric materials, should satisfy special requirements caused by orthopedic surgery: biocompatibility, strength, durability, adhesion, osseointegration [9,10]. Polymeric materials should be durable to an aggressive environment during a sterilization process as well as have no toxic components in the compound during the usage of implant [3,4,8]. The modern thermoplastics could be easily manufactured, that allow creating implants with complicated shapes, and it is very suitable for personalized endoprosthetics. Most thermoplastic polymers don't cause an immune response, which is one of the criteria of biocompatibility [11]. However, during the usage of implant, several polymeric materials may release toxic monomers [8]. Surfaces of the most thermoplastic polymers are usually bioinert [12], that create difficulties for recovering of around laid tissues [13]. The bioinert property of thermoplastics lead to adhesion failure of the implant or the prosthesis with around laid tissues. As a result, additional surgery may be required [2]. Finally, thermoplastic implants and prosthesis have a long-lasting manufacturing cycle.

Today, the possibilities of thermosetting polymers usage in endoprosthetics have not been studied yet and represent scientific novelty [14–16]. That is due to special features of such thermosetting polymers, particularly the liquid-solid state transition during its curing, which leads to almost impossible full monomer conversation. This will lead to the presence of a small amount of residual unreacted toxic monomer around laid tissues. Another unpleasant feature concerns the necessity to precisely control the linking density of the thermosetting polymers, since a highly linked polymer matrix has the brittle failure behavior [17]. However, such limitations of the thermosetting polymers could be overcome by different methods of modification of their chemical composition, for example: an introduction of chain extensions to increase the plastic deformation of the polymer matrix; a selection of monomers and catalysts that increase conversion. It is safety to say that high speed between monomers shortens the time of manufacturing for

medical devices. The great advantage of thermosetting polymer matrix consists in high adhesion to various surfaces due to generation of chemical and physical bonding.

The main purpose of this research consists in investigation of the physical, chemical and surface properties of available biocompatible thermoplastics in order to determine requirements to chemical composition of thermosetting polymer matrix for satisfying special requirements caused by orthopedic surgery. Well known experimental methods (FTIR, DTA/TG, DSC, XRD and SEM) were used to determine the physical, chemical and surface properties of investigated thermoplastics [18–21].

Materials and Methods

In this article as the object of research several biocompatible (by the standard ISO 10993 USP Class VI according to the data provided by the manufacturer on the official website [22]) thermoplastic polymers are considered: polyacrylonitrile-co-butadiene-co-styrene (ABS-M30i, Stratasys Ltd.), polycarbonate (PC-ISO, Stratasys Ltd.) and polyetherimide (Ultem 1010 Resin, Stratasys Ltd.).

Samples manufacturing

The standard samples were manufactured with the industrial grade 3D-printer Stratasys Fortus 450mc (Stratasys Ltd.) by fused deposition modeling. 3D-printing is realized by a print head with 2 nozzle tips. The angle of thread laying was close to 90° during 3D-printing. The 3D-printing surface is presented by a plastic build sheet, which is held to the aluminum platen with a machined pattern using a vacuum source. The thickness of the one layer for ABS-M30i and PC-ISO was 178 μm, whereas the thickness of the one layer of Ultem 1010 Resin was 254 μm due to technological limitations of the 3D-printer. The thickness of each sample was 3 mm. 3D-printing was performed in a heated build chamber. The temperature of the chamber was around 88–105 °C, while the speed of 3D-printing was about 6–7.5 mm/sec.

Fourier-transform infrared spectroscopy

Fourier-transform infrared (FTIR) spectra were obtained by the spectrometer IRTracer-100 (Shimadzu Europa GmbH) using the attenuated total reflectance (ATR) console Quest (Specac Ltd.). Diamond was used as the crystal material. The incidence angle of the IR-beam on the crystal surface was 45°. The penetration depth was 2 μm. The FTIR spectroscopy was conducted in order to identify chemical structure, confirm data declared by the manufacturer and check the absence of additional chemical modification.

Contact angle measurement

Static and dynamic contact angles were measured with the goniometer KRUSS DS225 (KRUSS GmbH) using Advance software. Static contact angles were measured by the sessile drop method with drop volume about 2–4 μl. The contact angle values were averaged between 5–10 measurements at different points of the surface. Dynamic contact angles were measured by a method of increasing and decreasing drop volume that is being in contact with the surface. Firstly, 4 μl were placed at the surface of the

polymers, wherein the syringe tip stayed in the drop. Advancing contact angle was obtained during simultaneously adding the following 6 μl with measuring of contact line increasing. The receding contact angle was obtained by the contact line decreasing during removal of the liquid.

Differential thermal and thermogravimetric analysis

For the differential thermal and thermogravimetric analysis, the derivatograph DTG-60 (Shimadzu Europa GmbH) was used. Samples with 11 ± 1 mg mass were placed in an alumina crucible and heated from 20 to 600 °C with 10 °C/min speed in the air environment. The empty alumina crucible was used as a comparison sample.

Differential scanning calorimetry

The glass temperature (*T*g) of polymers were obtained by differential scanning calorimeter (DSC) Netzsch DSC 214 Polyma (Netzsch GmbH). Samples with 10.5 ± 2.5 mg mass were placed in an alumina crucible with pierced lid and heated from 50 to 250 °C with 10°C/min speed in the N_2 environment in accordance with ISO 11357-1:2016. The DSC curve of empty alumina crucible, heated at the same conditions, was subtracted from all obtained DSC curves.

Distilled water and blood plasma absorption

The distilled water and blood plasma adsorption was measured in accordance with ISO 62:2008. In case of distilled water, the investigation was conducted at 23 °C with a 10-day duration of the exposition. In case of blood plasma, the investigation was conducted also at 23 °C but with an 8-day duration of the exposition.

X-ray diffraction

Wide-angle X-ray diffraction (XRD) data were obtained by Rigaku Corporation SmartLab 3 (Rigaku Americas Corp.) diffractometer using CuK_α radiation equipped with a nickel foil filter. $K_ß$ was not considered due to using nickel filter. The length of the emitted wave by the copper tube of the apparatus equals 1.54 Å. Samples were pre-cleaned and placed in a non-crushed state in a measuring cuvette. Data were obtained by counting for 2 s at each 0.01° step in 2θ. The blank curve was subtracted from all obtained data. Determination of interplanar distance with separation of peaks was performed using the Origin 2019 software. Obtained curves were pre-smoothed by 80 points using the Fourier transform.

Scanning electron microscopy

The cross-section of polymers was obtained using scanning electron microscopy (SEM) by TESCAN VEGA 3 SBH (TESCAN Ltd.) microscope. Accelerated voltage was about 5 – 20 kV, focus distance was 15 mm and probe current was 17 pA. Samples were frozen in liquid N_2, cracked, and fixed on a double-sided tape. The carbon layer with 5 – 20 nm thickness was sprayed on the sample surface using the Q150RE (Quorum Technologies Ltd.). For an image registration, the secondary electron detector was used.

Results and Discussion

The FTIR spectroscopy

The IR-spectra of ABS-M30i (Fig. 1) contains absorption bands of –C–H– groups at 2924–2852, 1453 and 1267 cm^{-1}. Absorption bands at 1735 and 1267–1031 cm^{-1} indicate the presence of ester and ether groups. The presence of a styrene fragment is indicated by absorption bands 3060–3026, 1735, 1602, 1496, and 758–693 cm^{-1}. Absorption bands at 963–910 cm^{-1} indicate the presence of polybutadiene fragments. The presence of –CN fragments of an acrylonitrile is indicated by the absorption band at 2238 cm^{-1}. Absorption band at 3082 cm^{-1} indicates the presence of the aryl or of –C=C– groups. The absence of absorption bands near 3300, 1637 and 1552 cm^{-1}, which are typical for –NH– groups of amides, indicates on absence of antistatic agents, which are usually added in a commercial polyacrylonitrile-co-butadiene-co-styrene [23].

The IR-spectra of PC-ISO (Fig. 2) contains absorption bands of $-CH_3$ and $-CH_2-$ groups at 2967–2849 and 1413–1363 cm^{-1}. Absorption bands at 3050, 1602, 1500, 1465, and 760 cm^{-1} indicate the presence of aryl and *p*-substituted aryl rings. The presence of aryl-aryl, aryl-alkyl and alkyl-alkyl –C–O–C– ether groups is indicated by absorption bands at 1220–1012 cm^{-1}.

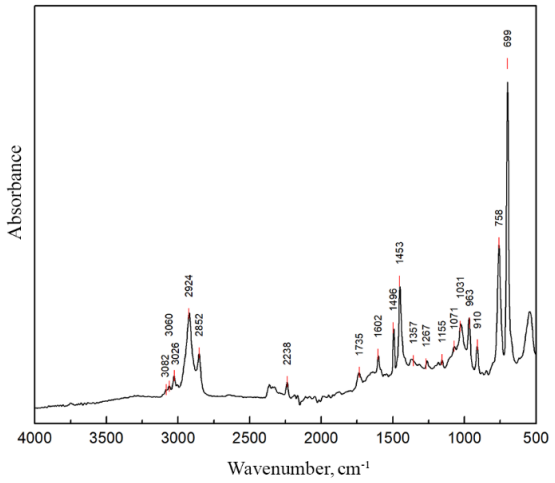

Fig. 1. The IR-spectra of ABS-M30i

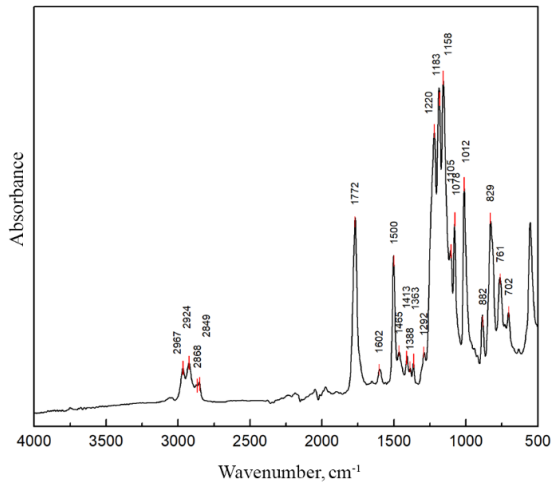

Fig. 2. The IR-spectra of PC-ISO

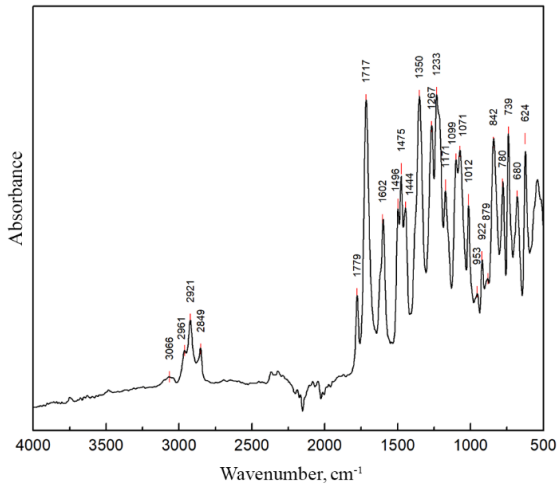

Fig. 3. The IR-spectra of Ultem 1010 Resin

More complicated the IR-spectra of Ultem 1010 Resin (Fig. 3) contains absorption bands of aryl ring at 3066 and 1602–1496 cm^{-1}, carbonyl groups of imide at 1717 cm^{-1} and –C(O)–N–C(O) – ring of imide at 1350, 1171, 1071, 842, and 739 cm^{-1}. The presence of ester groups is indicated by the absorption band at 1779 cm^{-1}. Absorption bands at 1267–1233, 1091 and 1012 indicate the presence of aryl-aryl and alkyl-aryl groups. The presence of $-CH_3$ and $-CH_2-$ groups is indicated by absorption bands at 2961–2849 and 953–922 cm^{-1} [24–26].

The investigation of wetting parameters

Surfaces of all investigated thermoplastics have transition or hydrophobic properties (Table 1), which leads to increasing persistence to an infection occurring [27]. At the same time the protein adhesion that leads to recovery of around laid tissues, could be shortened because of the hydrophobic property of the thermoplastics [3,28]. Ultem 1010 Resin has the largest contact angle hysteresis, which indicates high water adhesion to its surface. PC-ISO has the least contact angle hysteresis and ABS-M30i has the value between other thermoplastic polymers. However, all investigated thermoplastics have relatively high contact angle hysteresis, which may provide an increase of both proteins and bacterial adhesion [29,30]. Also, the blood plasma has high wettability of PC-ISO and Ultem 1010 Resin surfaces.

Table 1. The values of contact angles and hysteresis of all investigated thermoplastics

Thermoplastic	θ_W, °	θ_{Adv}, °	θ_{Rec}, °	Hysteresis θ, °	θ_P, °
ABS-M30i	89.6 ± 2.3	95.6 ± 0.6	24.4 ± 3.3	71.2 ± 3.9	92.1 ± 2.3
PC-ISO	89.5 ± 2.8	85 ± 1	22.6 ± 3.2	62.4 ± 4.1	84.7 ± 1.6
Ultem 1010 Resin	96.4 ± 3.1	103 ± 1.4	8.8 ± 1.2	94.2 ± 2.5	86.1 ± 2.9

DTA/TG and DSC investigations

All investigated thermoplastics have the same mass losing character (Fig. 4). The destruction temperature of ABS-M30i and PC-ISO (Fig. 4(a,b)) is about 375 °C. Ultem 1010 Resin is the most stable to oxidative destruction thermoplastic polymer, which starts to destruct at almost 500 °C (Fig. 4(c)). Ultem 1010 Resin loses about 2.5 wt. % of its mass up to 250 °C due to evaporation of volatile components. Weight loss may be caused by evaporation of the sorbed water from the sample, which is retained by hydrogen bonding between water molecules and amide groups of Ultem 1010 Resin. The same phenomena do not occur for ABS-M30i and PC-ISO.

All presented DSC curves include a single glass transition, which indicates the absence of crystal structure of all investigated thermoplastics (Fig. 5). Based on this study, it can be assumed that the investigated thermoplastics are amorphous. The glass transitions of ABS-M30i, PC-ISO and Ultem 1010 Resin equal 101.4, 135.8 and 207.2 °C.

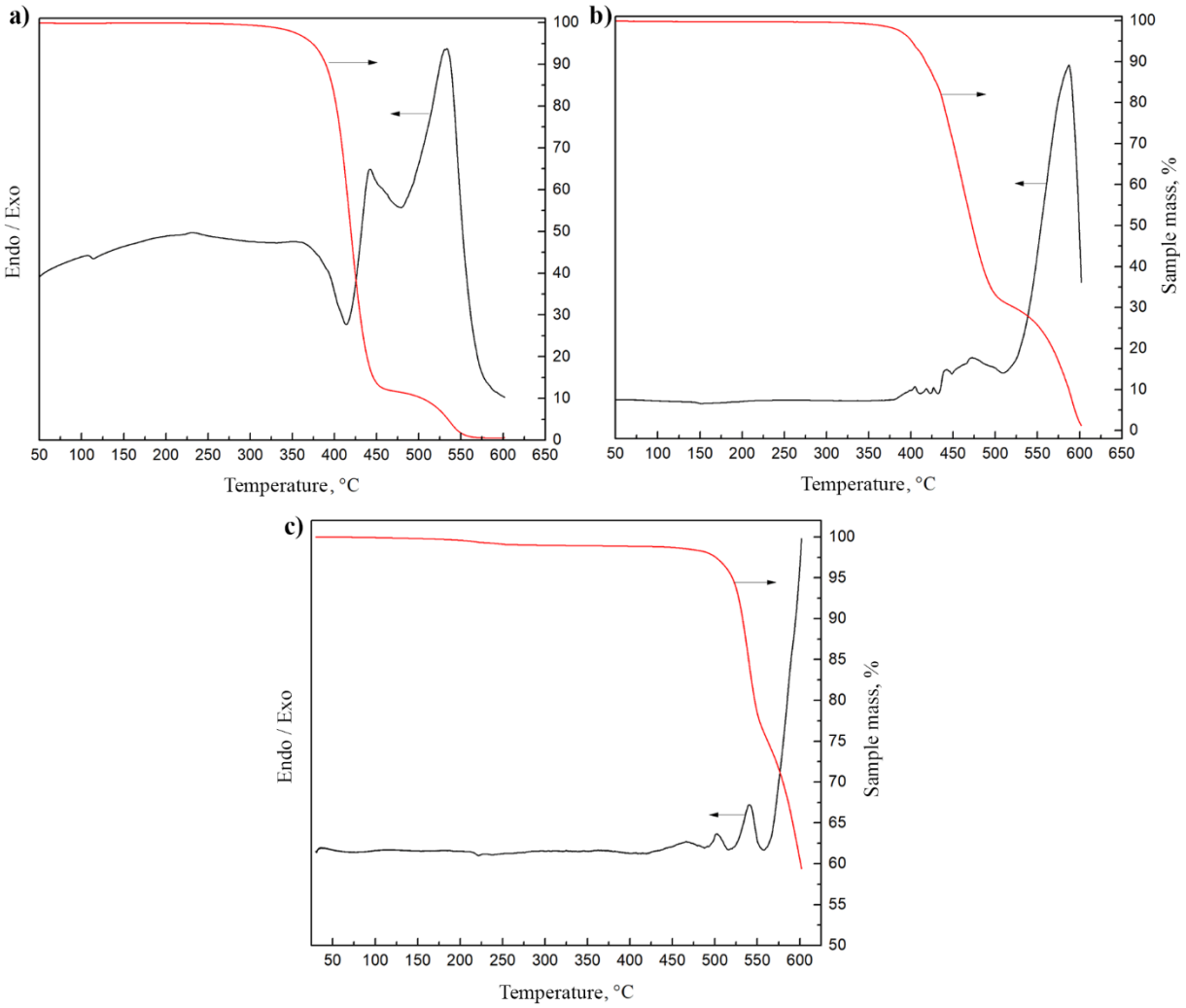

Fig. 4. DTA/TG curves: (a) ABS-M30i; (b) PC-ISO; (c) Ultem 1010 Resin

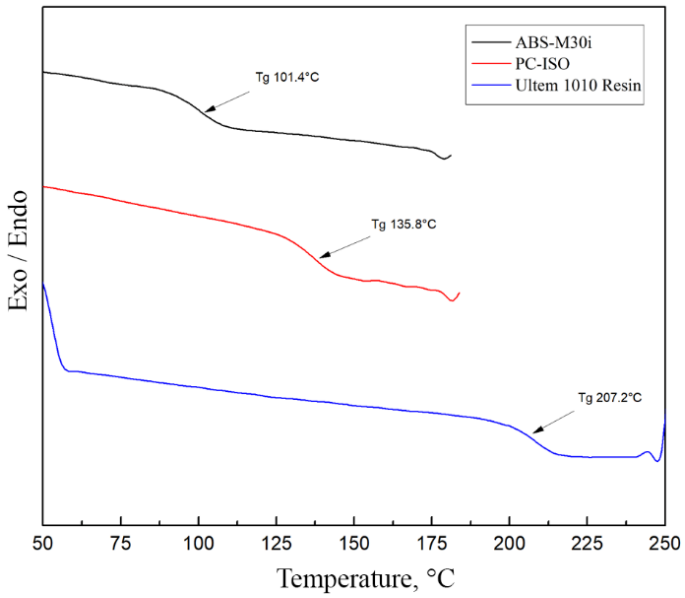

Fig. 5. DSC cooling curves of all investigated thermoplastics

Absorption investigation

It is well known that polymers tend to absorb surrounding substances. The amount of absorbed substance indicates the presence of open micropores or channels inside the polymer body or structure defects. It also may indicate the absence of water-soluble monomers. The absence of monomers in the final polymer is extremely important, since the toxicity of monomers significantly exceeds the toxicity of polymers. Moreover, the absorption of such substances can lead to undesirable both size changing and releasing components due to swelling. Since implants and prosthesis are not surrounded by the water, it would be useful to investigate behavior of thermoplastic polymers in bioliquids, for example blood plasma.

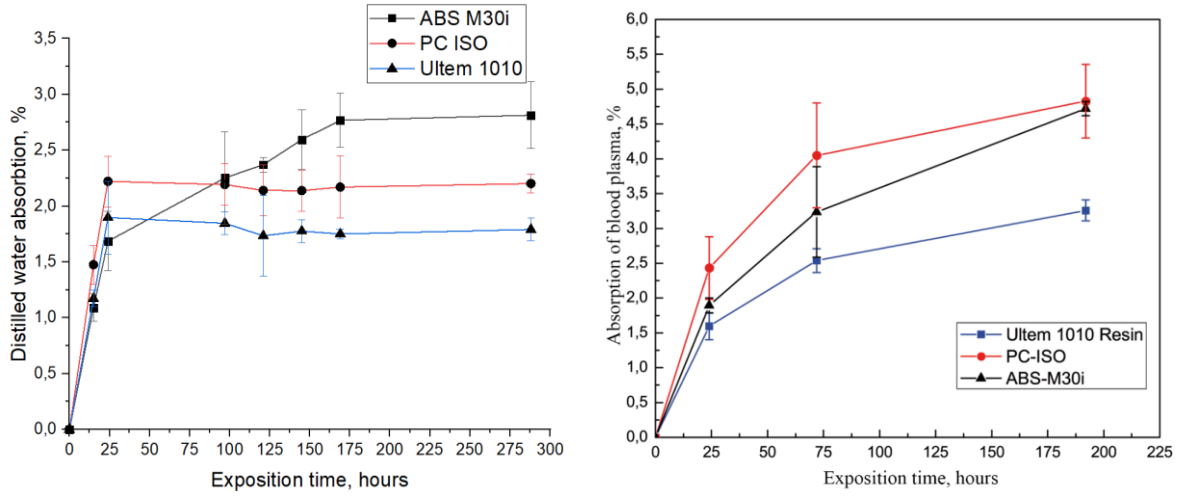

(a) (b)

Fig. 6. The dependence of the distilled water (a) and blood plasma (b) absorption versus exposition time

It was expected that the hydrophobic property of thermoplastic polymers in relation to the distilled water and blood plasma will lead to decreasing of their adsorption. However, all investigated thermoplastic samples tend to adsorb water (Fig. 6(a)), and the value of water uptake depends precisely on chemical structure and doesn't depend on wetting parameters. Thus, ABS-M30i demonstrates the highest distilled water adsorption, which equals 2.8 % after 190 hours of exposition. At the same time, Ultem 1010 Resin has the lowest distilled water absorption, which equals only 1.7 % after 190 hours of exposition. In addition, despite the relatively high value of the θ_P of ABS-M30i (Table 2), the value of blood plasma absorption after 190 hours is more than 4.5 wt. % (Fig. 6(b)). PC-ISO has the less value of the θ_P compared to ABS-M30i. However, the value of the absorbed blood plasma of PC-ISO is close to ABS-M30i. Ultem 1010 Resin has the least value of the blood plasma absorption (lower than 3 wt. %). Thus, the distilled water and blood plasma adsorption tightly correlate with the glass transition. Increasing glass temperature leads to decreasing liquid absorption. It is also well known that glass temperature tightly correlates with the number of chemical or physical bonds. Therefore, using a polymer matrix with relatively high cross-linking density (high glass temperature) leads to reduction of bioliquids adsorption.

Table 2. The values of distilled water and blood plasma adsorption of all investigated thermoplastics

Thermoplastic	Distilled water adsorption after 190 hours, %	Blood plasma adsorption after 190 hours, %
ABS-M30i	3.12	4.83
PC-ISO	2.17	4.72
Ultem 1010 Resin	1.66	3.26

Wide-angle XRD investigations

XRD has been successfully used to study various aspects of polymer structures, which include thermoplastics, thermosetting polymers and liquid crystalline polymers [31]. The supposition of amorphous structure of all investigated thermoplastic polymers also was confirmed by the XRD results (Figs. 8–10), since narrow peaks are absent in all diffraction patterns. It should be mentioned that mineral fillers are not detected in all investigated thermoplastic samples. It is possible to detect wide peaks (17–22 °C) layered on the broad polymer halo signal using the Levenberg-Marquardt algorithm, which is widely used for curve fitting. Corresponding 2Θ values are presented in Table 3. In addition, according to Bragg's law, Table 3 shows calculated values of d-space – the distances between polymer chains, which tend to form a low ordered structure, due to intermolecular orientational interactions [32].

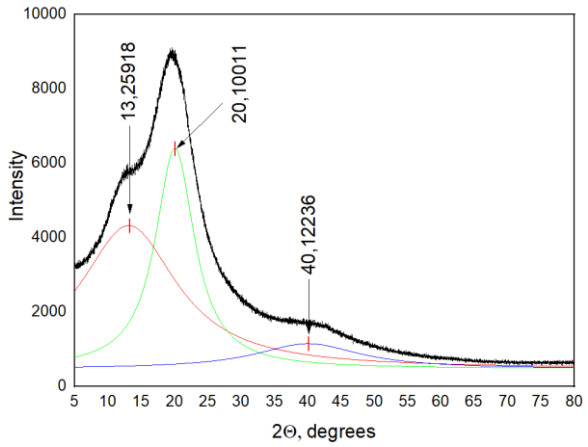

Fig. 8. Wide-angle XRD curve of ABS-M30i

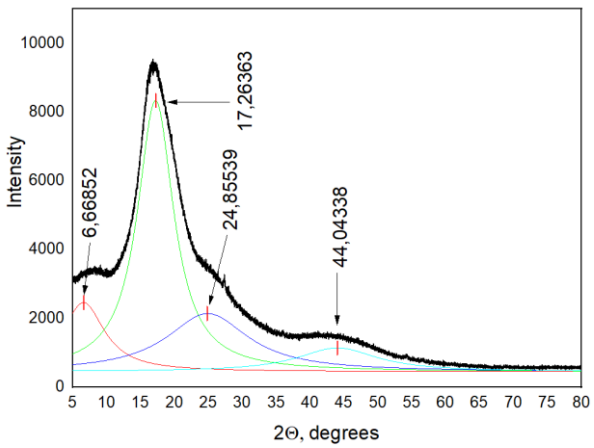

Fig. 9. Wide-angle XRD curve of PC-ISO

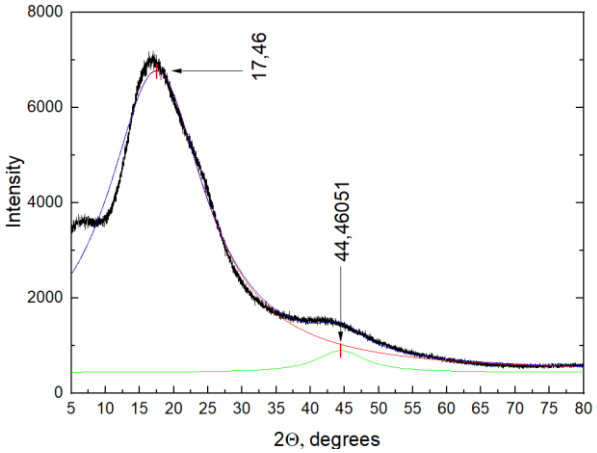

Fig. 10. Wide-angle XRD curve of Ultem 1010 Resin

Table 3. Interplane distance of all investigated thermoplastics

Thermoplastic	2Θ, °	d-space, Å
ABS-M30i	13.26	4.38
	20.1	2.2
	40.12	3.53
PC-ISO	6.66	13.25
	17.26	5.11
	24.86	3.55
	44.04	2
Ultem 1010 Resin	17.46	5.05
	44.46	1.98

SEM investigation of the cross-section

The cross-sections of ABS-M30i (Fig. 11(a)) and PC-ISO (Fig. 11(b)) contain trays of plastic deformation, whereas the cross-section of Ultem 1010 Resin is smooth and typical for a brittle failure (Fig. 11(c)). Pores lower than 10 μm are absent, whereas pores larger than 50 μm are presented at all images. Such structure is the result of the sample manufacturing with 3D-printing by fused deposition modeling and can facilitate the osseointegration [28].

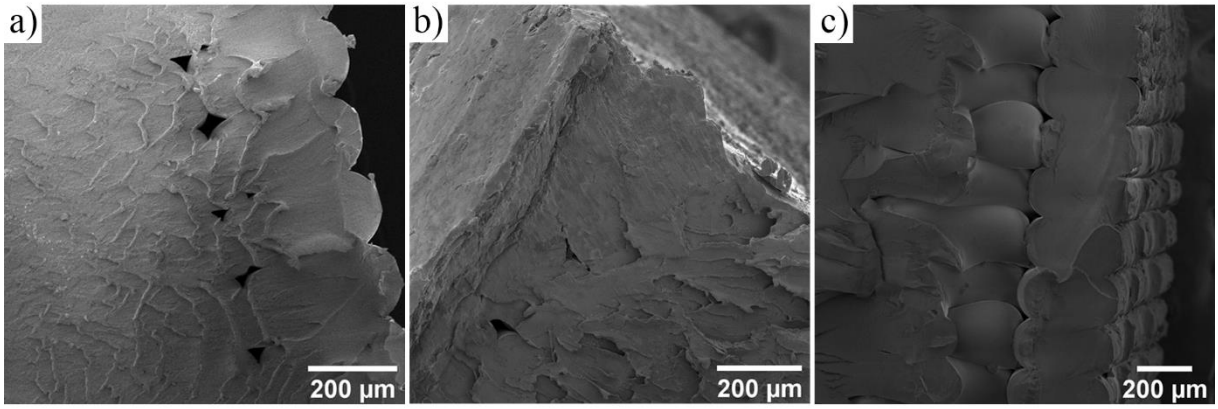

Fig. 11. The cross-section of thermoplastic samples after several cycles of loading: (a) ABS-M30i; (b) PC-ISO; (c) Ultem 1010 Resin

Conclusion

This paper focuses on experimental determination of physical, chemical and surface properties of several biocompatible thermoplastics: ABS-M30i (polyacrylonitrile-co-butadiene-co-styrene), PC-ISO (polycarbonate) and Ultem 1010 Resin (polyetherimide). Investigated samples were manufactured with the industrial grade 3D-printer by fused deposition modeling. In particular, the following physical, chemical and surface properties were obtained: IR-spectra, static and dynamic contact angles, DTA/TG curves, DSC curves, dependence of the distilled water and blood plasma absorption versus exposition time, wide-angle XRD curves, cross-section of samples after several cycles of loading.

For further research it is important to outline suggestions to chemical composition of thermosetting polymer matrix for satisfying orthopedic surgery requirements. Physical

and mechanical properties of thermosetting polymers may be varied by controlling the proportion of "hard" and "soft" blocks, which can be presented by block-copolymers. For example, aromatic ethers, alicyclic ethers and polyimides can be used as "hard" segments of thermosetting polymer matrix. While the demanding "soft" behavior of the whole thermosetting polymer matrix can be achieved by integration of long-chain polyurethanes or oligoether epoxy resins or derivatives of polyethylene terephthalate or derivatives of polycarbonate. It is quite desirable to include polar groups in thermosetting polymer, which will facilitate wettability of surfaces and increase adhesion. A special attention should be paid to the inclusion of mineral fillers in such polymers, since it may affect physical, chemical and surface properties.

References

1. Mamalis AG, Ramsden JJ, Grabchenko AI, Lytvynov LA, Filipenko VA, Lavrynenko SN. A novel concept for the manufacture of individual sapphire-metallic hip joint endoprostheses. *Journal of Biological Physics and Chemistry*. 2002;6(3): 113–118.
2. Grace EP, Webster TJ. A review of nanotechnology for the development of better orthopedic implants. *Journal of Biomedical Nanotechnology*. 2005;1(1): 18–29.
3. Mishra S, Chowdhary R. Peek materials as an alternative to titanium in dental implants: A systematic review. *Clinical Implant Dentistry and Related Research.* 2019;21(1): 208–222.
4. Venkata PM, Lecka-Czernik B, Ebraheim NA, Jayasuriya AC. An overview of recent advances in designing orthopedic and craniofacial implants. *Journal of Biomedical Materials Research Part A*. 2013;101(11): 3349–3364.
5. Borovkov AI, Maslov LB, Zhmaylo MA, Zelinskiy IA, Voinov IB, Keresten IA, Mamchits DV, Tikhilov RM, Kovalenko AN, Bilyk SS, Denisov AO. Finite element stress analysis of a total hip replacement in two-legged standing. *Russian Journal of Biomechanics*. 2018;22(4): 382–400. (In Russian)
6. Keresten IA, Borovkov AI, Zhmaylo MA, Kovalenko AN, Bilyk SS. Finite element modeling and stress analysis of hip components in two-legged standing. In: *Science week SPbPU: proceedings of the international scientific conference. Institute of applied mathematics and mechanics*. St. Petersburg: Polytechnic University Publishing; 2016. p.74–76. (In Russian)
7. Keresten IA, Sudneva AI. Finite element analysis of the effective properties of the lattice structure of the implant. In: *Science week SPbPU: proceedings of the international scientific conference. Institute of applied mathematics and mechanics.* St. Petersburg: POLITEKh-PRESS Publishing; 2018. p.329–332. (In Russian).
8. Eschbach LY. Nonresorbable polymers in bone surgery. *Injury*. 2000;31: D22–D27.
9. Shastri VP. Non-degradable biocompatible polymers in medicine: past, present and future. *Current Pharmaceutical Biotechnology*. 2003;4(5): 331–337.
10. Kumar N, Bharti A, Kumar A, Kushwaha RK, Patel KK. Nanomaterials coating for bio-implant applications: a re-analysis. *Materials Physics and Mechanics*. 2023;51(6): 92–106.
11. Asghari F, Samiei M, Adibkia K, Akbarzadeh A, Davaran S. Biodegradable and biocompatible polymers for tissue engineering application: a review. *Artificial Cells, Nanomedicine, and Biotechnology*. 2017;45(2): 185–192.
12. Oladapo BI, Zahedi SA, Ismail SO, Omigbodun FT, Bowoto OK, Olawumi MA, Muhammad MA. 3D printing of PEEK–cHAp scaffold for medical bone implant. *Bio-Design and Manufacturing*. 2021;4(1): 44–59.
13. Teo AJT, Mishra A, Park I, Kim Y-J, Park W-T, Yoon Y-J. Polymeric biomaterials for medical implants and devices. *ACS Biomaterials Science & Engineering*. 2016;2(4): 454–472.
14. Raquez JM, Deléglise M, Lacrampe MF, Krawczak P. Thermosetting bio(materials) derived from renewable resources: A critical review. *Progress in Polymer Science*. 2010;35(4): 487–509.
15. Zaokari Y, Persaud A, Ibrahim A. Biomaterials for adhesion in orthopedic applications: A review. *Engineered Regeneration*. 2020;1: 51–63.
16. Bashandeh K, Amiri A, Rafieerad A, Rahman S, Yan W, Dhingra S, Polycarpou AA. MXene-aromatic thermosetting copolyester nanocomposite as an extremely wear-resistant biocompatible implant material for osteoarthritis applications. *Applied Surface Science*. 2022;600: 154124.
17. Song HB, Baranek A, Worrell BT, Cook WD, Bowman CN. Photopolymerized triazole-based glassy polymer networks with superior tensile toughness. *Advanced Functional Materials*. 2018;28(22): 1801095.

18. Kobykhno IA, Kuznetcov DA, Didenko AL, Smirnova VE, Vaganov GV, Ivanov AG, Popova EN, Litvinova LS, Svetlichnyi VM, Vasilyeva ES, Tolochko OV, Yudin VE, Kudryavtsev VV. Multiblock copoly(urethane-amide-imide)s with the properties of thermoplastic elastomers. *Materials Physics and Mechanics*. 2018;40(2): 221–230.
19. Mohd Idrus MAM, Hamdan S, Rahman MdR, Islam MdS. Liquefied tropical wood/ polypropylene composites: preparation and physico-mechanical properties. *Materials Physics and Mechanics*. 2011;11(2): 126–136.
20. Hassan MF, Noruddin N. The effect of lithium perchlorate on poly (sodium 4-styrenesulfonate): studies based on morphology, structural and electrical conductivity. *Materials Physics and Mechanics*. 2018;36(1): 8–17.
21. Pearson A. *Are FDM materials biocompatible?* Available from: https://www.stratasys.com/en/resources/blog/fdm-materials-biocompatability/ [Accessed 11th July 2024].
22. Slonov AL, Zhansitov AA, Rzhevskaya EV, Khakulova DM, Khashirova SYu. On the plasticization on highly-filled polyphenylene sulfone. *Materials Physics and Mechanics*. 2019;42(5): 535–543.
23. Desrousseaux C, Cueff R, Aumeran C, Garrait G, Mailhot-Jensen B, Traoré O, Sautou V. Fabrication of acrylonitrile-butadiene- styrene nanostructures with anodic alumina oxide templates, characterization and biofilm development test for staphylococcus epidermidis. *PloS one*. 2015;10(8): e0135632.
24. Yang CP, Su YY, Chen YC. Colorless poly (ether-imide) s deriving from 2, 2-bis [4-(3, 4-dicarboxyphenoxy) phenyl] propane dianhydride (bpada) and aromatic bis (ether amine) s bearing pendent trifluoromethyl groups. *European Polymer Journal*. 2006;42(4): 721–732.
25. Liu Y, Xing Y, Zhang Y, Guan S, Zhang H, Wang Y, Wang Y, Jiang Z. Novel soluble fluorinated poly (ether imide) s with different pendant groups: synthesis, thermal, dielectric, and optical properties. *Journal of Polymer Science Part A: Polymer Chemistry*. 2010;48(15): 3281–3289.
26. Kiefer J, Fries J, Leipertz A. Experimental vibrational study of imidazolium-based ionic liquids: Raman and infrared spectra of 1-ethyl-3- methylimidazolium bis (trifluoromethylsulfonyl) imide and 1-ethyl-3-methylimidazolium ethylsulfate. *Applied Spectroscopy*. 2007;61(12): 1306–1311.
27. Zhukovskii VA, Filipenko TS, Sukovatykh BS, Valuiskaya NM. Polymeric endoprostheses for reconstructive–restorative surgery. *Fibre Chemistry*. 2018;50(3): 219–225.
28. Menzies KL, Jones L. The impact of contact angle on the biocompatibility of biomaterials. *Optometry and Vision Science*. 2010;87(6): 387–399.
29. Górecka Z, Teichmann J, Nitschke M, Chlanda A, Choińska E, Werner C, Święszkowski W. Biodegradable fiducial markers for x-ray imaging–soft tissue integration and biocompatibility. *Journal of Materials Chemistry B*. 2016;4(34): 5700–5712.
30. Doll K, Fadeeva E, Schaeske J, Ehmke T, Winkel A, Heisterkamp A, Chichkov BN, Stiesch M, Stumpp NS. Development of laser-structured liquid-infused titanium with strong biofilm-repellent properties. *ACS Applied Materials & Interfaces*. 2017;9(11): 9359–9368.
31. Murthy NS, Minor H. General procedure for evaluating amorphous scattering and crystallinity from X-ray diffraction scans of semicrystalline polymers. *Polymer*. 1990;31(6): 996–1002.
32. Guo WF, Chung TS. Study and characterization of the hysteresis behavior of polyimide membranes in the thermal cycle process of pervaporation separation. *Journal of Membrane Science*. 2005;235(1–2): 13–22.

About Authors

Daniil A. Erofeev
PhD Student (St. Petersburg Institute of Technology (Technical University), St. Petersburg, Russia)

Pavel B. Pirozhnikov
Candidate of Chemical Sciences
Senior Lecturer (St. Petersburg Institute of Technology (Technical University), St. Petersburg, Russia)

Ilya A. Keresten
Candidate of Technical Sciences
Associate Professor (Peter the Great St. Petersburg Polytechnic University, St. Petersburg, Russia)

Alexey G. Titov
Candidate of Medical Sciences
Head of the Department (Institute of Medical Education of Almazov National Medical Research Centre, St. Petersburg, Russia)